

A transition to elasto-viscoplastic turbulence in inertialess channel flow?

James Shemilt* and Neil J. Balmforth

Department of Mathematics, University of British Columbia, Vancouver, BC, V6T 1Z2, Canada

Duncan R. Hewitt

*Department of Applied Mathematics and Theoretical Physics,
University of Cambridge, Wilberforce Road, Cambridge CB3 0WA, UK*

(Dated: June 30, 2026)

We conduct 2D numerical simulations employing a widely used constitutive law for elasto-viscoplastic fluids to show that linear instability leads to spatio-temporal complexity in inertialess channel flow. Fluctuations in the final state are pronounced near and between the yield surfaces that border an unyielded plug spanning the centre of the channel. The instability and transition arise for Weissenberg numbers of order unity and higher.

Yield-stress fluids flow only when subjected to a sufficiently large stress, deforming like solids below that critical threshold. Such materials are commonplace in geophysical, biological and industrial settings [1, 2]. Many yield-stress fluids deform viscoelastically both below and above the yield stress, and recent modelling studies have focused on characterizing elastic effects in 3D printing [3, 4], airway mucus flows [5], bubble dynamics [6–9], particle transport and sedimentation [10, 11] and thinning fluid threads [12, 13].

A number of constitutive laws have been proposed to capture ‘elasto-viscoplastic’ material behaviour [2, 14]. The most widely used is Saramito’s law [15, 16], which switches at the yield stress between a Kelvin-Voigt viscoelastic solid and an Oldroyd-B-type viscoelastic fluid. The predictions of the Saramito model for simple Couette flows have been compared with rheometric measurements, with a mix of agreement and some setbacks [14, 17]. The widespread adoption of this model in computational studies of various complex flow problems motivates the current study, in which we re-examine a simpler problem: pressure-driven channel flow.

For this flow configuration, recent work [18] has pointed out notable consequences of adopting the Saramito model. In particular, a novel linear instability was discovered at zero Reynolds number, suggesting that elasto-viscoplastic rheology may introduce significant complexity even in a relatively simple flow. A range of uni-directional base flows were found to be unstable, with the awkward feature that the shortest streamwise wavelengths have the highest growth rates. However, those base states could also develop discontinuities in the normal stresses and shear rate as they evolved from their initial state. Such discontinuities present a significant challenge in linear stability analysis, leading [18] to retreat to a high-Weissenberg-number limit to simplify the problem, obscuring the generality of the results. In this Letter, with the aid of fully nonlinear, 2D numerical simulations covering a range of Weissenberg numbers, we assess this elasto-viscoplastic linear instability more generally and explore its consequences on the nonlinear flow

dynamics.

For viscoelastic fluids without a yield stress, linear instabilities can trigger complex, or even chaotic, dynamics at zero Reynolds number. Commonly, these instabilities are associated with curved streamlines [19, 20], and the same mechanism has been identified in elasto-viscoplastic flows [21, 22]. On the other hand, Wilson & Rallison [23] discovered an inertialess linear instability in rectilinear channel flow of highly shear-thinning viscoelastic fluid, which was later suggested to underscore the complex flow patterns in experiments [24, 25]. However, although purely elastic turbulence is possible in inertialess channel flow of Oldroyd-B fluid [26–28], the laminar flow is linearly stable, except at high solvent viscosities and Weissenberg numbers [29, 30]. By contrast, we demonstrate here that linear instability triggers spatio-temporal complexity in inertialess elasto-viscoplastic channel flow without requiring extreme solvent viscosities or Weissenberg numbers, merely moderate elasticity and a yield stress. The complex dynamics are crucially connected with the presence of unyielded plugs in the flow.

Model— We consider the flow of an elasto-viscoplastic fluid down a 2D channel of width \mathcal{H} , driven by a pressure gradient $-\Gamma$. We express the governing equations in dimensionless form, scaling lengths by \mathcal{H} , stresses and pressure by $\frac{1}{2}\Gamma\mathcal{H}$, velocities by $U = \frac{1}{2}\Gamma\mathcal{H}^2/(\mu_p + \mu_s)$, and time by \mathcal{H}/U , where μ_p and μ_s are polymeric and solvent viscosities, respectively. Assuming incompressibility and zero inertia, mass and momentum balance then imply

$$\nabla \cdot \mathbf{u} = 0, \quad \nabla p = \beta \nabla^2 \mathbf{u} + \nabla \cdot \boldsymbol{\tau} + 2, \quad (1)$$

for the velocity $\mathbf{u} = (u, v)$, pressure p , polymer stress, $\boldsymbol{\tau}$, and viscosity ratio, $\beta = \mu_s/(\mu_p + \mu_s)$, describing the channel geometry in terms of the Cartesian coordinates (x, y) . We write Saramito’s constitutive law [15] as

$$W \overset{\nabla}{\boldsymbol{\tau}} + \max\left(1 - \frac{B}{\tau}, 0\right) \boldsymbol{\tau} = (1 - \beta) \dot{\boldsymbol{\gamma}} + \kappa \nabla^2 \boldsymbol{\tau}, \quad (2)$$

where $\overset{\nabla}{\boldsymbol{\tau}}$ is the upper convected derivative [31], $\tau = \sqrt{(\tau_{xx} - \tau_{yy})^2 + 4\tau_{xy}^2}$ is the polymer stress invariant, and

shear rates are given by $\dot{\gamma} = \nabla \mathbf{u} + (\nabla \mathbf{u})^T$. As standard in many viscoelastic flow simulations [32–34], polymer stress diffusion is included to ease numerical computation, with coefficient κ . The dimensional parameters are the Weissenberg number, $W = \lambda U / \mathcal{H}$, Bingham number, $B = 4\tau_Y / \Gamma$, κ and β , where λ is the fluid relaxation time and τ_Y is the yield stress. At the channel walls, $y = \pm \frac{1}{2}$, we impose no slip or penetration and no-flux conditions on τ .

Solution methods— We solve (1) and (2) in a periodic domain $0 \leq x \leq L$, generally taking $L = \frac{\pi}{2}$. We use the open-source spectral solver Dedalus [35] with $N_x = 256$ Fourier modes and $N_y = 384$ Chebyshev modes to discretize in space, and a time step of $dt = 10^{-3}$ or smaller. We also conducted tests with $(N_x, N_y) = (384, 512)$ and the time step halved, with no significant impact on the results. Simulations are run until $t = t_{\text{end}} = 1000$. We take $\beta = 0.5$, representing moderate solvent viscosity, and set $\kappa = 10^{-5}$ to avoid substantial stress diffusion whilst maintaining adequate spatial resolution. To explore viscoelastic effects and their interplay with the yield stress, we vary W while fixing $BW^{-1} = \frac{1}{2}$, which ensures that the unyielded fraction of fluid in the channel is comparable between each simulation. We separately compute unidirectional base-flow solutions using centred finite differences on a uniform grid to approximate derivatives in y , integrating in time using MATLAB’s ode15s solver.

Initial conditions— As initial conditions, we adopt $(\tau_{xx}, \tau_{xy}, \tau_{yy}) = (a_0 + 10^{-3}B \sin(2\pi x/L), 0, 0)$, taking $a_0 = 0$ to simulate evolution from no initial polymer stress, or $a_0 = B$ to explore the effect of a polymeric pre-stress that fully yields fluid. The introduction of a uniform extensional stress is not meant to mimic any specific flow preparation, but is chosen for simplicity, and generates base flows that differ from those without any pre-stress, with impact on the linear stability [18]. The addition of a wavy perturbation facilitates the exploration of instabilities growing with a specific wavelength, and the subsequent emergence of complex dynamics with richer spatial structure. Note that the initial state is symmetrical about the centreline of the channel; this symmetry is maintained throughout the simulation. We have also run simulations in which initial stresses are initialized with small-amplitude random noise instead; solutions then lose symmetry about $y = 0$, but otherwise we find qualitatively similar dynamics.

Unidirectional base flows— Without stress diffusion, the x -independent base flows predicted by the model equations are not unique [18]: the final state depends on the initial stress configuration, here corresponding to $(\tau_{xx}, \tau_{xy}, \tau_{yy}) = (a_0, 0, 0)$. Solutions for our two representative cases of a_0 are illustrated in Fig. 1; the final states reached without diffusion are shown by dashed lines. When $a_0 = 0$, an unyielded plug develops in the centre of the channel, buffered from the walls by layers of yielded fluid. Discontinuities in normal stress and shear

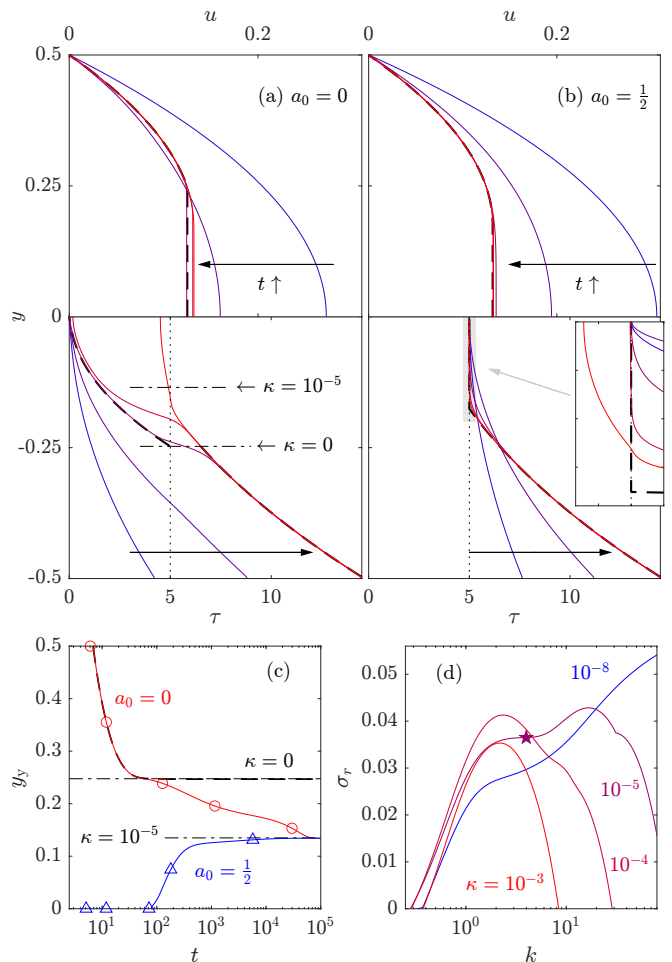


FIG. 1. (a,b) Unidirectional flow solutions (solid lines) with $(W, B, \beta, \kappa) = (10, 5, 0.5, 10^{-5})$ and (a) $a_0 = 0$ and (b) $a_0 = 0.5$, at the five times indicated by circles and triangles in (c) (and colour-coded, from blue to red, and as indicated by arrows). The velocity u is shown in the upper half of the channel; the stress invariant τ over the lower half (with a magnification inside the shaded region shown by the inset panel in (b)). (c) Yield surface position, $y_y(t)$, for the solutions in (a) (red) and (b) (blue). Dashed lines in (a-c) show the late-time solutions with $\kappa = 0$, and dot-dashed lines indicates the final yield surface positions. (d) Growth rates of the most unstable mode from linear theory for the final base state with stress diffusion for the values of κ indicated; the star marks the growth rate for $(k, \kappa) = (4, 10^{-5})$.

rate develop across the yield surfaces $y = \pm y_y$, the locations where τ increases through B . By contrast, for $a_0 = B$, the stresses and shear rates remain continuous and a marginally yielded ‘pseudo-plug’ forms across the centre of the channel, over which τ always slightly exceeds B . Other states are possible for different choices of a_0 [18], but here we focus on the two cases in Fig. 1, which provide convenient settings in which to explore the flow dynamics.

The base-flow solutions pictured in Fig. 1 become adjusted by stress diffusion: for $a_0 = 0$, diffusion smooths

the sharp stress gradients developing at the yield surfaces. Nevertheless, at intermediate times ($t < 100$), the solution with $\kappa = 10^{-5}$ matches that without diffusion. Over longer times, stress diffusion across the yield surfaces has greater impact, causing the diffusive solution to diverge from its non-diffusive counterpart, with y_y drifting nearer the channel's centre (Fig. 1(c)). Diffusion is less significant for the solution with $a_0 = B$ because sharp stress gradients no longer develop. However, diffusion permits the stress invariant to fall below B at late, but finite times. A fraction of the pseudo-plug of the non-diffusive problem then becomes unyielded. The final diffusive adjustments of the two solutions take place for times of $O(\kappa^{-1})$, eventually bringing both to the same final state (*cf.* Fig. 1(c)).

Linear instability— Stress discontinuities in non-diffusive base flows pose a significant challenge to conducting linear stability analysis [18]. The final steady states reached with diffusion are continuous, however, permitting their stability to be analysed in detail. Key results are illustrated in Fig. 1(d) for normal-mode perturbations with dependence $e^{ikx+\sigma t}$, where k is the wavenumber and $\sigma = \sigma_r + i\sigma_i$ the (complex) growth rate. For the lowest values of κ , growth rates are highest at the largest wavenumbers, as found for $\kappa = 0$ [18]. Stronger stress diffusion reduces the growth rates for high k , introducing a preferred wavenumber. Lower wavenumbers are, instead, destabilized by polymer diffusion, a result stemming mostly from diffusive adjustments at the yield surfaces of the base state. This destabilization is not equivalent to the polymer-diffusion instability found for viscoelastic fluids [32, 33], which arises at the walls and was not observed in our elasto-viscoplastic problem.

For $\kappa = 10^{-5}$, the growth rate in Fig. 1(d) is maximized across a wide range of wavenumbers, $1 \lesssim k \lesssim 50$. This range motivates the choice $L = \frac{\pi}{2}$ for our simulations, so that wavy perturbations with $k = 4$ grow in a domain that is sufficiently long for shorter wavelengths to also emerge.

Nonlinear dynamics— Fig. 2 presents results from simulations of our two examples with $a_0 = 0$ and $a_0 = 5$. The symmetry of the solutions about the centreline is exploited to compactly display snapshots of the evolving stress invariant τ and streamwise velocity perturbations $u - \bar{u}$, where an overbar denotes streamwise average: $\bar{f} = L^{-1} \int_0^L f \, dx$.

Focusing first on the case with $a_0 = 0$, the evolution begins with a short transient adjustment from the initial configuration towards a state resembling the corresponding base-flow solution, with a plug spanning the centre of the channel (Fig. 2(a), $t = 100$). However, small-amplitude fluctuations are present with wavelength $\frac{\pi}{2}$, seeded by the initial perturbation to τ_{xx} . We gauge the strength of those fluctuations by an amplitude $A(t)$, defined as the root mean square of $\tau - \bar{\tau}$, which is plotted in Fig. 2(c). This amplitude grows exponentially in time,

until about $t = 200$. Thereafter, $A(t)$ saturates, and a nonlinear wave emerges that is localized around, and significantly deforms, the yield surfaces (Fig. 2(a), $t = 250$).

For later times, $A(t)$ oscillates irregularly about an approximately constant level A_{end} . Simultaneously, shorter wavelengths emerge in the spatial structure (*cf.* $t = 500, 800$), as illustrated by multiple streaks in the stress field and fingers of unyielded fluid protruding into the central plug. Occasionally, stresses fall back below B along those fingers, isolating unyielded pockets within the plug (*e.g.* $t = 800$). Over this late-time phase of evolution, fluctuations remain strongest near and between the yield surfaces (Fig. 2(d)). The excitation of a broad range of streamwise spatial scales is illustrated further in Fig. 2(e). Shown are spectra of τ extracted by averaging Fourier transforms in x over later times and two representative intervals of y : region *I* embeds fully yielded fluid near the wall; region *II* encompasses the migrating yield surface and unyielded core of the channel (see (d)). For region *II*, the spectrum decreases as k^{-1} at low wavenumbers, before steepening closer to k^{-4} at higher wavenumbers; the spectrum is significantly lower over region *I*.

With a pre-stress that initially yields the fluid, the initial stages of evolution are somewhat different (Fig. 2(b)): although the stress remains close to B across the centre of the channel (*cf.* Fig. 1(b)), several spatially structured plugs form as τ drops below B , driven by x -varying stresses. The plugs expand as unstable perturbations again grow exponentially with time; the growth rate matches that predicted by the stability analysis of the long-time diffusive base flow (the star in Fig. 1). By $t = 250$, $A(t)$ again saturates (Fig. 2(c)), but the unyielded plug adopts a different structure than in the $a_0 = 0$ simulation. In particular, thin bands of strongly yielded fluid protrude through the centreline, fracturing the plug.

At later times, the two simulations become more similar: by $t = 500$, multiple streaks again appear in the stress field, complicating the yield surfaces and highlighting the excitation of shorter wavelengths. Again, flow perturbations are mostly localized near and between the yield surfaces. The stress across the unyielded plug also significantly decreases, to the extent that the cross-stream average and spectra of τ now become more comparable between the two simulations (Fig. 2(d,e)). Nevertheless, the two cases differ in finer detail, the history of the stress being buried in the elastic memory of the plugged regions. The ultimate stress state also remains unclear because the simulations do not run to times comparable to that required for stress diffusion across the plug, $t = O(\kappa^{-1})$.

Finally, in [18], it was observed that linear instability became suppressed at smaller Weissenburg numbers, although the analysis was limited to base states with pseudo-plugs. To examine this conclusion more gener-

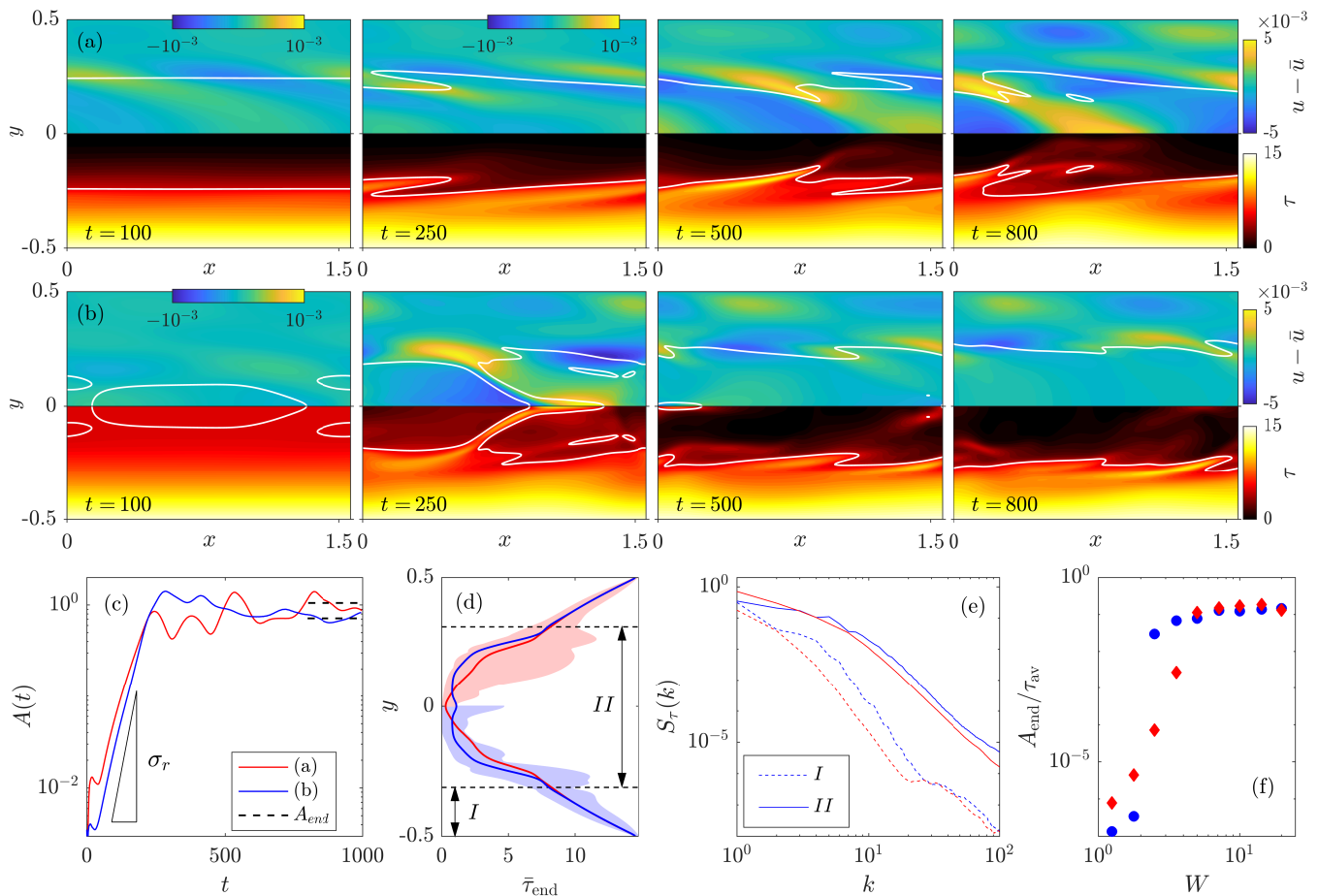


FIG. 2. (a) Snapshots of $u - \bar{u}$ and τ over the upper or lower halves of the channel, respectively, from a 2D numerical simulation with $(W, B, \beta, a_0, L) = (10, 5, \frac{1}{2}, 0, \frac{\pi}{2})$ at the times indicated (the full solutions are symmetrical about the centreline). Solid white lines indicate the yield surfaces where $\tau = B$. (b) A similar set of plots to those in (a) but for a simulation with $a_0 = 5$. (c) Time series of fluctuation amplitude $A(t)$; dashed lines show the mean value A_{end} over $800 < t < 1000$. The triangle indicates the linear growth rate shown as a star in Fig. 1. (d) The spread of the stress invariant τ over x and t plotted against y for the same time interval (shaded regions, with the simulation in (a) in the upper half of the channel and that in (b) in the lower half), together with the average $\bar{\tau}_{end}$ (solid lines). (e) $S_\tau(k)$, streamwise Fourier spectra (the magnitude of the Fourier transform in x of τ), averaged over $800 < t < 1000$ and the windows of y indicated in (d), labelled I (dashed; yielded wall region) and II (solid; plug-like central region). In (c-e), the simulations from (a) and (b) are shown by red or blue lines, respectively. (f) Final amplitude A_{end} relative to the final average stress τ_{av} for a suite of simulations with varying W and $(B, \beta, L) = (\frac{1}{2}W, \frac{1}{2}, \frac{\pi}{2})$, with $a_0 = 0$ (blue circles) or $a_0 = B$ (red diamonds).

ally, we conducted suites of simulations with varying W , taking $B = \frac{1}{2}W$ and the same values as before for the remaining parameters. The late-time amplitudes A_{end} for each simulation are shown in Fig. 2(f). For $W = 2.5$, the case with $a_0 = 0$ is stable, whereas instability and transition occurs with $a_0 = B$. At lower W , the initial sinusoidal perturbation decays in time, both with and without pre-stress. For $W \geq 5$, both suites of simulations exhibit instability, with similar A_{end} for the two cases of a_0 . Evidently, moderate Weissenberg numbers are required for instability, and the impact of applying a uniform extensional pre-stress on the resulting complex spatio-temporal dynamics is relatively minor.

Discussion— In this Letter, we have demonstrated

that linear instability leads to the creation of a complex flow state in inertialess channel flow, for an elasto-viscoplastic fluid described by Saramito’s model. Spatio-temporal complexity is focused near and between the yield surfaces, linking its emergence with unyielded plug-like flow. The temporal variability and broad range of spatial scales of the final state lead one to speculate that the instability might be capable of triggering a transition to ‘elasto-viscoplastic turbulence’, by analogy with viscoelastic flow dynamics [36].

Our predictions should be confronted by experiments with elasto-viscoplastic fluids. If confirmed, we may have established a new pathway to complex flow dynamics in inertialess channel flow, driven by an interplay between

elasticity and viscoplasticity. If, instead, there is disagreement with experiments, then we expose a significant deficiency in the most popular elasto-viscoplastic constitutive model, that drives spurious dynamics in moderately elastic fluids.

Acknowledgements— We thank Theo Lewy, Hugo França, Rich Kerswell, Maziyar Jalaal and Mark Martinez for discussions, suggestions and assistance in implementing the Dedalus code.

Data availability— Data are available upon reasonable request from the authors.

* shemilt@math.ubc.ca

- [1] N. J. Balmforth, I. Frigaard, and G. Ovarlez, Yielding to stress: Recent developments in viscoplastic fluid mechanics, *Ann. Rev. Fluid Mech.* **46**, 121 (2014).
- [2] P. Coussot, Fifty shades of yield stress fluids: rheological challenges and engineering perspectives, *Rheol. Acta* **64**, 167 (2025).
- [3] H. L. França, M. Jalaal, and C. M. Oishi, Elasto-viscoplastic spreading: From plastocapillarity to elasto-capillarity, *Phys. Rev. Research* **6**, 013226 (2024).
- [4] H. Franca, D. Tieman, J. Shemilt, C. Oishi, and M. Jalaal, Coalescence of printed yield stress filaments in direct ink writing, Pre-print, arXiv:2601.09870 (2026).
- [5] O. Erken, B. Fazla, M. Muradoglu, D. Izbassarov, F. Romanò, and J. B. Grotberg, Effects of elastoviscoplastic properties of mucus on airway closure in healthy and pathological conditions, *Phys. Rev. Fluids* **8**, 053102 (2023).
- [6] V. Sanjay, D. Lohse, and M. Jalaal, Bursting bubble in a viscoplastic medium, *J. Fluid Mech.* **922**, A2 (2021).
- [7] A. G. Balasubramanian, V. Sanjay, M. Jalaal, R. Vinuesa, and O. Tammisola, Bursting bubble in an elasto-viscoplastic medium, *J. Fluid Mech.* **1001**, A9 (2024).
- [8] P. Moschopoulos, A. Spyridakis, S. Varchanis, Y. Dimakopoulos, and J. Tsamopoulos, The concept of elasto-visco-plasticity and its application to a bubble rising in yield stress fluids, *J. Non-Newton. Fluid Mech.* **297**, 104670 (2021).
- [9] A. Kordalis, G. Esposito, P. Zakeri, Y. Dimakopoulos, and J. Tsamopoulos, Mass transfer effects during bubble mobilisation in yield stress fluids via pressure reduction, *J. Fluid Mech.* **1031**, A18 (2026).
- [10] D. Fraggedakis, Y. Dimakopoulos, and J. Tsamopoulos, Yielding the yield-stress analysis: a study focused on the effects of elasticity on the settling of a single spherical particle in simple yield-stress fluids, *Soft matter* **12**, 5378 (2016).
- [11] E. Chaparian, M. N. Ardekani, L. Brandt, and O. Tammisola, Particle migration in channel flow of an elastoviscoplastic fluid, *J. Non-Newton. Fluid Mech.* **284**, 104376 (2020).
- [12] P. Zakeri, P. Moschopoulos, Y. Dimakopoulos, and J. Tsamopoulos, Scaling analysis and self-similarity near breakup of elasto-viscoplastic liquid threads under creeping flow, *J. Fluid Mech.* **1020**, A37 (2025).
- [13] J. Shemilt and N. Balmforth, Rayleigh-plateau instability of an elasto-viscoplastic filament, Pre-print, arXiv:2512.21059 (2026).
- [14] D. Fraggedakis, Y. Dimakopoulos, and J. Tsamopoulos, Yielding the yield stress analysis: A thorough comparison of recently proposed elasto-visco-plastic (evp) fluid models, *Journal of Non-Newtonian Fluid Mechanics* **236**, 104 (2016).
- [15] P. Saramito, A new constitutive equation for elastoviscoplastic fluid flows, *J. Non-Newton. Fluid Mech.* **145**, 1 (2007).
- [16] P. Saramito, A new elastoviscoplastic model based on the Herschel–Bulkley viscoplastic model, *J. Non-Newton. Fluid Mech.* **158**, 154 (2009).
- [17] K. Kamani, G. J. Donley, and S. A. Roger, Unification of the rheological physics of yield stress fluids, *Phys. Rev. Lett.* **126**, 218002 (2021).
- [18] J. Shemilt, N. Balmforth, and D. Hewitt, Start-up and inertialess instability in elasto-viscoplastic channel flow, Pre-print, arXiv:2606.01010 (2026).
- [19] P. Pakdel and G. H. McKinley, Elastic instability and curved streamlines, *Phys. Rev. Lett.* **77**, 2459 (1996).
- [20] S. S. Datta, A. M. Ardekani, P. E. Arratia, A. N. Beris, I. Bischofberger, G. H. McKinley, J. G. Eggers, J. E. López-Aguilar, S. M. Fielding, A. Frishman, *et al.*, Perspectives on viscoelastic flow instabilities and elastic turbulence, *Phys. Rev. Fluids* **7**, 080701 (2022).
- [21] M. Mousavi, Y. Dimakopoulos, and J. Tsamopoulos, Elasto-visco-plastic flows in benchmark geometries: I. 4 to 1 planar contraction, *J. Non-Newton. Fluid Mech.* **327**, 105218 (2024).
- [22] M. Mousavi, Y. Dimakopoulos, and J. Tsamopoulos, Elasto-visco-plastic flows in benchmark geometries: II. flow around a confined cylinder, *J. Non-Newton. Fluid Mech.* **336**, 105384 (2025).
- [23] H. J. Wilson and J. M. Rallison, Instability of channel flow of a shear-thinning White–Metzner fluid, *J. Non-Newton. Fluid Mech.* **87**, 75 (1999).
- [24] H. Bodiguel, J. Beaumont, A. Machado, L. Martinie, H. Kellay, and A. Colin, Flow enhancement due to elastic turbulence in channel flows of shear thinning fluids, *Phys. Rev. Lett.* **114**, 028302 (2015).
- [25] R. Poole, Elastic instabilities in parallel shear flows of a viscoelastic shear-thinning liquid, *Phys. Rev. Fluids* **1**, 041301 (2016).
- [26] M. Lellep, M. Linkmann, and A. Morozov, Purely elastic turbulence in pressure-driven channel flows, *Proc. Nat. Acad. Sci. USA* **121**, e2318851121 (2024).
- [27] M. Beneitez, J. Page, Y. Dubief, and R. R. Kerswell, Transition route to elastic and elasto-inertial turbulence in polymer channel flows, *Phys. Rev. Fluids* **9**, 123302 (2024).
- [28] G. Foggi Rota, C. Amor, S. Le Clainche, and M. E. Rosti, Unified view of elastic and elasto-inertial turbulence in channel flows at low and moderate reynolds numbers, *Phys. Rev. Fluids* **9**, L122602 (2024).
- [29] M. Khalid, V. Shankar, and G. Subramanian, Continuous pathway between the elasto-inertial and elastic turbulent states in viscoelastic channel flow, *Phys. Rev. Lett.* **127**, 134502 (2021).
- [30] G. Buza, J. Page, and R. R. Kerswell, Weakly nonlinear analysis of the viscoelastic instability in channel flow for finite and vanishing reynolds numbers, *J. Fluid Mech.* **940**, A11 (2022).
- [31] R. B. Bird, R. C. Armstrong, and O. Hassager, Dynamics of polymeric liquids. vol. 1: Fluid mechanics, (1986).

- [32] M. Beneitez, J. Page, and R. R. Kerswell, Polymer diffusive instability leading to elastic turbulence in plane couette flow, *Physical Review Fluids* **8**, L101901 (2023).
- [33] M. Beneitez, S. Mrini, and R. R. Kerswell, Linear instability in planar viscoelastic taylor–couette flow with and without explicit polymer diffusion, *Journal of Non-Newtonian Fluid Mechanics* , 105459 (2025).
- [34] T. A. Lewy, S. M. Fielding, P. D. Olmsted, and R. R. Kerswell, Elastic turbulence in highly entangled polymers and wormlike micelles, *Phys. Rev. Lett.* **136**, 104001 (2026).
- [35] K. J. Burns, G. M. Vasil, J. S. Oishi, D. Lecoanet, and B. P. Brown, Dedalus: A flexible framework for numerical simulations with spectral methods, *Phys. Rev. Research* **2**, 023068 (2020).
- [36] V. Steinberg, Elastic turbulence: an experimental view on inertialess random flow, *Annual Review of Fluid Mechanics* **53**, 27 (2021).